Rheological behaviors and viscosity prediction model of cementitious composites with various carbon nanotubes

Li, Hongyan; Li, Zhenming; Qiu, Liangsheng; Dong, Sufen; Ouyang, Jian; Dong, Xufeng; Han, Baoguo

DOI
10.1016/j.conbuildmat.2023.131214

Publication date
2023

Document Version
Final published version

Published in
Construction and Building Materials

Citation (APA)
Li, H., Li, Z., Qiu, L., Dong, S., Ouyang, J., Dong, X., & Han, B. (2023). Rheological behaviors and viscosity prediction model of cementitious composites with various carbon nanotubes. *Construction and Building Materials*, *379*, Article 131214. https://doi.org/10.1016/j.conbuildmat.2023.131214

Construction and Building Materials 379 (2023) 131214

Contents lists available at ScienceDirect

Construction and Building Materials

journal homepage: www.elsevier.com/locate/conbuildmat

Rheological behaviors and viscosity prediction model of cementitious composites with various carbon nanotubes

Hongyan Li [a], Zhenming Li [b], Liangsheng Qiu [c], Sufen Dong [d,*], Jian Ouyang [d], Xufeng Dong [e], Baoguo Han [c,*]

[a] State Key Laboratory of High Performance Civil Engineering Materials, Jiangsu Sobute New Materials Co., Ltd, Nanjing 211103, China
[b] Department of Materials and Environment (Microlab), Faculty of Civil Engineering and Geoscience, Delft University of Technology, Delft 2628 CN, the Netherlands
[c] School of Civil Engineering, Dalian University of Technology, Dalian 116024, China
[d] School of Transportation and Logistics, Dalian University of Technology, Dalian 116024, China
[e] School of Material Science and Engineering, Dalian University of Technology, Dalian 116024 China

ARTICLE INFO

Keywords:
Carbon nanotubes
Cementitious composites
Rheology
Viscosity
Model

ABSTRACT

This study aims to understand the effects and mechanisms of length, diameter, and functional group of carbon nanotubes (CNTs) on rheological behaviors of cementitious composites. The experimental results show that the addition of CNTs decreases the flow index and increases the critical shear rate of cementitious composites. CNTs with a sub-micrometer length and small diameter endow cementitious composites with high yield stresses and minimum viscosities. Influenced by the high water absorption of hydroxylic groups, the minimum viscosity of cementitious composites with hydroxyl functionalized CNTs is larger than that of composites with pristine carbon nanotubes (p-CNTs). By contrast, the yield stress and minimum viscosity of cementitious composites with carboxyl functionalized CNTs are smaller than that of cementitious composites with p-CNTs at most contents due to the high dispersion induced by carboxyl groups. The effect mechanisms of CNTs on rheological behaviors can be attributed to adsorption effect and entanglement effect, which are closely related to length, diameter and functionalization groups of CNTs. The established minimum viscosity prediction model considering the influence of CNT physicochemical features can provide guidance for regulating the workability and hardened performance of CNTs modified cementitious composites.

1. Introduction

Owing to their excellent physical and mechanical properties, carbon nanotubes (CNTs) are favorable nano-fillers for cementitious composites [1,2] and has received extensive attention from researchers and engineers [3,4]. For example, compressive, flexural, tensile, and splitting strengths of cementitious composites can be increased by 50 %, 269 %, 19 %, and 86 %, respectively [3,5,6], due to the addition of CNTs. Meanwhile, the incorporation of CNTs endows cementitious composites with excellent piezoresistive properties [7,8], electromagnetic interference shielding properties [9] and damping performances [10,11].

The rheological property of cementitious composites with CNTs plays a decisive role in the pumping power and pressure drop of concrete, and also has significant impact on the workability, homogeneity, mechanical properties and durability of concrete especially that with reinforcement bars12–16. Hence, it is important to investigate the influences of CNTs on the rheological properties of cementitious materials. At present, previous investigation mainly focus on the relationships between CNT content, dispersion agent and rheological parameters of cementitious composites. Leonavičius et al. [17] found that the content increasing of CNTs led to pH decrease of water solutions and viscosity increase of the fresh cement pastes. Meanwhile, low contents of CNTs (0.00005 %~0.005 %) decreases the dynamic viscosity of water solutions by approximately 15 % and high amounts of CNTs (0.05 % and 0.5 %) increases the dynamic viscosity of cement paste by 1.3 to 4.7 times [18]. Skripkiunas et al. [19] stated that the addition of 0.25 % multi-walled carbon nanotubes (MWCNTs) in cement paste decreases the yield stress by 30.7 % and increases the plastic viscosity by 29.6 %. Besides, some researchers focused on the effect of the surfactant on the rheological property of cement pastes with MWCNTs. Mendoza et al. [20] found that adding both MWCNTs and surfactant suspensions increases the yield stress and has little impact on viscosity of cement

* Corresponding authors.
E-mail addresses: dongsufen@dlut.edu.cn (S. Dong), hithanbaoguo@163.com (B. Han).

https://doi.org/10.1016/j.conbuildmat.2023.131214
Received 8 July 2022; Received in revised form 15 January 2023; Accepted 27 March 2023
Available online 5 April 2023

pastes, resulting from the triple interaction between MWCNT, surfactant, and cement. Skripkiunas et al. [19] showed that the combined using of polycarboxylate ether (PCE) and MWCNT suspension decreases the plastic viscosity of cement pastes by 9.90 %, and reduces the yield stress to 0 Pa, as well as endows cement paste with a shear-thinning behavior. De Paula et al. [21] grew CNTs directly onto the cement clinker and studied the influences of CNTs on rheological behaviors of cement pastes. The results showed that the addition of these CNTs has almost no influence on rheological behaviors of cement pastes.

It is worthwhile to note that the physicochemical features of CNTs have remarkable influence on the rheological behaviors of cement pastes. The physical characters, mainly including length and diameter, almost determines the dispersion and aggregation of CNTs in cement pastes. The hydrophilic ability of CNTs is improved by the presence of surface modification groups including hydroxyl and/or carboxyl groups, and then the water absorption capacity of CNTs in cement pastes is increased [22,23]. The change of dispersion state and water absorption capacity of CNTs will significantly change the rheological behavior of cement pastes. This leads to that the related results obtained by different researchers without considering the impact of CNTs' physicochemical features (i.e., length, diameter, and functionalization group) are not comparative. Therefore, the influence of CNTs' physicochemical features on rheological behaviors of cementitious composites should be investigated. Additionally, the workability of cementitious composites degrades significantly with the increasing CNT content. However, there is a lack of in-depth research on the prediction of the workability of cementitious composites with CNTs. Therefore, CNTs with different lengths, diameters, and functionalization groups were used to investigate the influences of CNT physicochemical features on the rheological behaviors of cement pastes in this study. The effect mechanisms of CNTs with different lengths, diameters, and functionalization groups were revealed and a viscosity prediction model was established to reveal the effect of CNT content on the workability of cement pastes.

2. Materials and experiments

2.1. Materials

The cement used in this study was P·O 42.5R purchased from Dalian Onoda Cement Co. ltd., China. The chemical compositions of the used cement are shown in Table 1. A polycarboxylate-based superplasticizer (SP), 3310C purchased from Dalian Sika Co., ltd., China, was used as water reducer. Three types of CNTs, including p-CNTs, hydroxyl functionalized CNT (CNT-OH), and carboxyl functionalized CNTs (CNT-COOH) were utilized. All the CNTs were ordered from Chengdu Organic Chemicals Co. ltd. The physical and chemical properties of CNTs are presented in Table 2.

Fig. 1 shows the smooth, complete, and multiple-walled structure of p-CNTs (LT, Lt, ST, St). Fig. 1(a), (b), and (c) exhibit the dispersion state of the four types of p-CNTs, among which LT has the most favorable dispersion state (Fig. 1(a)) and Lt has the worst dispersion state (Fig. 1 (c)). Additionally, the different diameter of CNTs can be distinguished in Fig. 1(d) (LT, outer diameter is around 22.08 nm, and inner diameter is around 6.94 nm) and Fig. 1(e) (St, outer diameter is around 9.47 nm, and inner diameter is around 3.17 nm), respectively.

Table 3 lists zeta potentials of CNTs. The high Zeta potential generate large repulsive force of CNTs, resulting in a relatively stable state of CNTs in cement pastes. The low Zeta potential causes small repulsive force between CNTs. Hence, CNTs with low Zeta potential is prone to aggregation. Table 3 shows that the absolute values of the zeta potential for CNTs (−29.9 mV ~ −20.0 mV) are much higher than those of cement particles (−10.4 mV) [24]. This will induce considerable electrostatic repulsion to overcome van der Waals' forces between CNTs and lead to a low aggregation degree [25]. That is to say, CNTs are more likely to adhere to cement particles rather than themselves [24].

The maximum values of water vapor adsorption (mg/g) at the same relative pressure ($P/P_0 = 0.90$) and temperature of 20 °C for CNTs are shown in Table 4. A larger water vapor adsorption of CNTs, representing the ability of the water absorption of CNT in the cement pastes is greater, leaves a less the free water in the cement pastes and the smaller the free activity space of CNTs, thus leading to the worse dispersion of CNTs. The water absorption capacities of CNTs with micrometer length and large diameter are larger than that of CNTs with sub-micrometer length and small diameter. CNTs with large special surface area (SSA) possess large water absorption capacities because they can provide more attachment points per unit mass for water. Furthermore, the CNT-OH can absorb more water compared with p-CNTs and CNT-COOH.

2.2. Paste preparation

A total of 8 types of cement pastes were prepared. For each type of cement paste, 5 contents (0.1 %, 0.3 %, 0.5 %, 0.7 %, and 1.4 % by volume of cement) of CNTs were investigated. The detailed mix proportions of cement pastes with/without CNTs are given in Table 5. The water-to-cement ratio (w/c) was fixed at 0.24, and the SP content was fixed at 1.0 % by the weight of cement.

CNTs are easily entangled in cementitious composites due to hydrophobicity and huge van der Waals force arising from the high polarizability [26] and large aspect ratio [27]. Uniform dispersion of CNTs is quite crucial for their effectiveness on performance of cementitious composites. The commonly used method for improving the dispersion state of CNTs include physical and chemical method. Sonication, as a typical physical dispersion method, is the most widely used technique to achieve a uniform dispersion of nanomaterial in various solutions through mechanical breaking up the clusters [28]. The addition of surfactants is a chemical method to uniformly disperse carbon nanofillers [25,29]. In this study, a combined method of ultrasonication and SP (a kind of surfactants) [25] was used to improve the dispersion of CNTs in cement paste.

The schematic diagram of the paste preparation is shown in Fig. 2. First, the SP was added to water with light shaking to prepare an SP solution. Then, different contents of CNTs were added to the SP solution followed by a sonication treatment for 1 h to prepare uniform CNT suspensions. After that, the CNT suspensions were cooled by the water bath to the ambient temperature. At last, cement particles were added into the CNT suspensions within 90 s. The paste was mixed by a stirring of 500 r/min for 2 min, and a speed of 60 r/min for another 1 min.

2.3. Rheological behavior test

The rheological behavior test was performed by an MCR 301 rheometer with a constant temperature of 25 ± 0.1 °C immediately after the cement paste preparation. The rheometer used is a coaxial cylinder, the rotor diameter of which is 26.657 mm, and the gap between the rotor and cylinder is 1.130 mm, as shown in Fig. 3(a). Three steps were set to conduct the rheological behavior test of cement pastes, as shown in Fig. 3(b). First, all samples were pre-sheared with 300 s^{-1} for 2 min to break down the flocculation structure. After that, a rest was applied to create a uniform and stable condition. Then, a speed-up step from 0 to 100 s^{-1} was set and finally followed by a ramp-down phase from 100 to

Table 1
Chemical components of P·O 42.5 R cement.

Composition	CaO	SiO_2	Al_2O_3	Fe_2O_3	SO_3	MgO	K_2O	TiO_2	Na_2O
wt. %	65	21.2	5.16	3.39	2.43	1.32	0.63	0.78	0.07

Table 2
Properties of CNTs.

Type	Outer diameter /nm	Inner diameter /nm	Length /μm	Aspect ratio (Length/ outer diameter, l/d)	–OH content /wt.%	–COOH content /wt.%	Specific surface area (SSA) /m^2/g
St	5 ~ 15	2 ~ 5	0.5 ~ 2	33 ~ 400	–	–	>350
ST	20 ~ 30	5 ~ 10	0.5 ~ 2	16 ~ 100	–	–	>120
StH	5 ~ 15	2 ~ 5	0.5 ~ 2	33 ~ 400	5.58	–	>380
StC	5 ~ 15	2 ~ 5	0.5 ~ 2	33 ~ 400	–	3.86	>270
Lt	5 ~ 15	2 ~ 5	10 ~ 30	667 ~ 6000	–	–	220 ~ 300
LT	20 ~ 30	5 ~ 10	10 ~ 30	333 ~ 1500	–	–	>110
LtH	5 ~ 15	2 ~ 5	10 ~ 30	667–6000	5.58	–	220 ~ 300
LtC	5 ~ 15	2 ~ 5	10 ~ 30	667 ~ 6000	–	3.86	220 ~ 300

Note: S and L denote short and long; t and T denote thin and thick; the thin CNTs were functionalized. H and C denote CNT with the surface functionalization groups of –OH and –COOH, respectively. Taking "StH" as an example, it represents short-thin CNTs with a functional group of –OH.

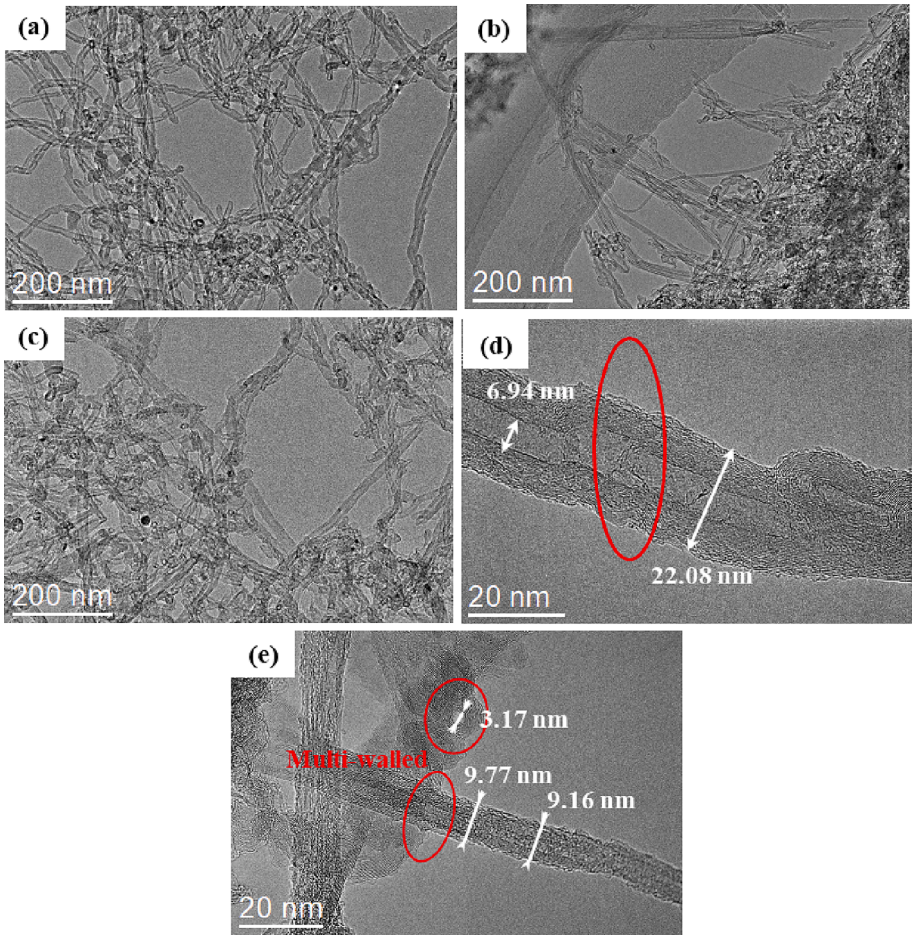

Fig. 1. TEM images of p CNTs: (a) low magnification images of LT, (b) Lt; (c) ST; (c) high magnification images of LT and (e) St.

Table 3
Zeta potential of CNTs (mV).

St	ST	StC	StH	Lt	LT	LtC	LtH
−20	−22.5	−29.9	−28.8	−26.2	−26	−22.7	−28

1 s^{-1}. Notably, three samples were prepared for each set.

3. Results and discussion

3.1. Rheological curves of cement pastes with CNTs

Fig. 4 shows typical curves of rheological behaviors of cement pastes with CNTs (take Lt as an example). Fig. 4(a) shows the shear stress-rate

Table 4
The maximum amounts of water vapor adsorption (mg/g).

St	ST	StC	StH	Lt	LT	LtC	LtH
320.899	124.122	339.75	432.385	389.45	118.321	368.88	451.384

Table 5
Mix proportions of cement paste with and without CNTs.

Sample	CNT (vol.%)	Cement
Control (C)	0	1
St-1/ST-1/Lt-1/LT-1/StH-1/StC-1/LtH-1/LtC-1	0.1	
St-3/ST-3/Lt-3/LT-3/StH-3/StC-3/LtH-3/LtC-3	0.3	
St-5/ST-5/Lt-5/LT-5/StH-5/StC-5/LtH-5/LtC-5	0.5	
St-7/ST-7/Lt-7/LT-7/StH-7/StC-7/LtH-7/LtC-7	0.7	
St-14/ST-14/Lt-14/LT-14/StH-14/StC-14/LtH-14/LtC-14	1.4	

Note: StH-1 denotes cement paste with 1 vol% StH.

curves of cement pastes with different contents of CNTs. It can be seen that the shear stress of cement pastes increases with the shear rate. Fig. 4 (b) shows the apparent viscosity-shear rate curves of cement pastes with different contents of CNTs. With the increasing shear rate, the apparent viscosity of cement pastes first decreases and then increase. There is a minimum viscosity in the shear rate region (0 ~ 100 s^{-1}).

Additionally, there are some commonalities of Fig. 4(a) and (b): (1) When CNT content is fixed, the error bar among the shear stresses/apparent viscosities are obvious at the low shear rate region (≤50 s^{-1}), while they are present slight differences at the high shear rate region (exceeds 50 s^{-1}) with the same CNT content. At the same time, the sensitivity of shear stresses/apparent viscosities of cement pastes with CNTs varies with the shear rate. (2) With the increase of CNT content, the shear stresses/apparent viscosities of cement pastes increase sharply at the low shear rate region, while they increase slightly at the high shear rate region. This means that the shear stresses/apparent viscosities of cement pastes with CNTs are more sensitive to the low shear rate compared with high shear rate.

These results are attributed to the aggregation of CNTs at low shear rate and good dispersion at high shear rate [30–32]. At a fixed shear rate, the shear stress/apparent viscosity increases with the CNT content, because the change of CNT content leads to the change of components (water, cement particles, and CNTs) in the cement paste. It can be attributed to the "adsorption effect" and "entanglement effect" of CNTs in cement pastes, which can be explained as follow:

(1) "Adsorption effect". The free water contributes to the fluidity of cement paste reduces due to the adsorption of CNTs (Fig. 4 (d)) with large SSA (Table 3) [25]. On the one hand, the distances between cement particles reduce, thus increasing the interface friction between cement particles. On the other hand, the distance between the CNTs decreases, and the number of direct bridges as well as entanglements between CNTs increases, resulting in the formation of flow-induced aggregations and clusters [33] and the increase of interface friction between cement particles. The above changes increase the shear stresses and apparent viscosities in the cement pastes.
(2) "Entanglement effect". Large content of CNTs is easily to form network structure due to their high flexibility and high aspect ratio [34–38]. When CNTs are added to cement pastes, part of

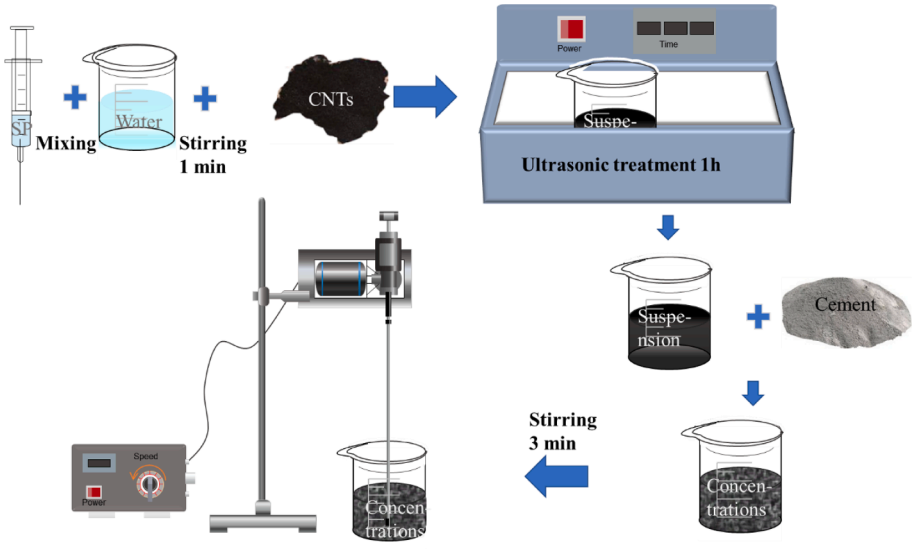

Fig. 2. Schematic diagram of preparation process for CNTs modified cement paste.

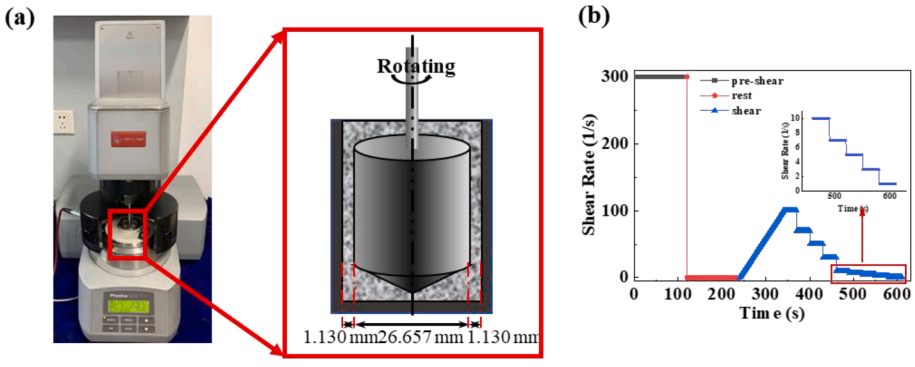

Fig. 3. Scheme of (a) coaxial cylinder rheometer and (b) shear rate steps.

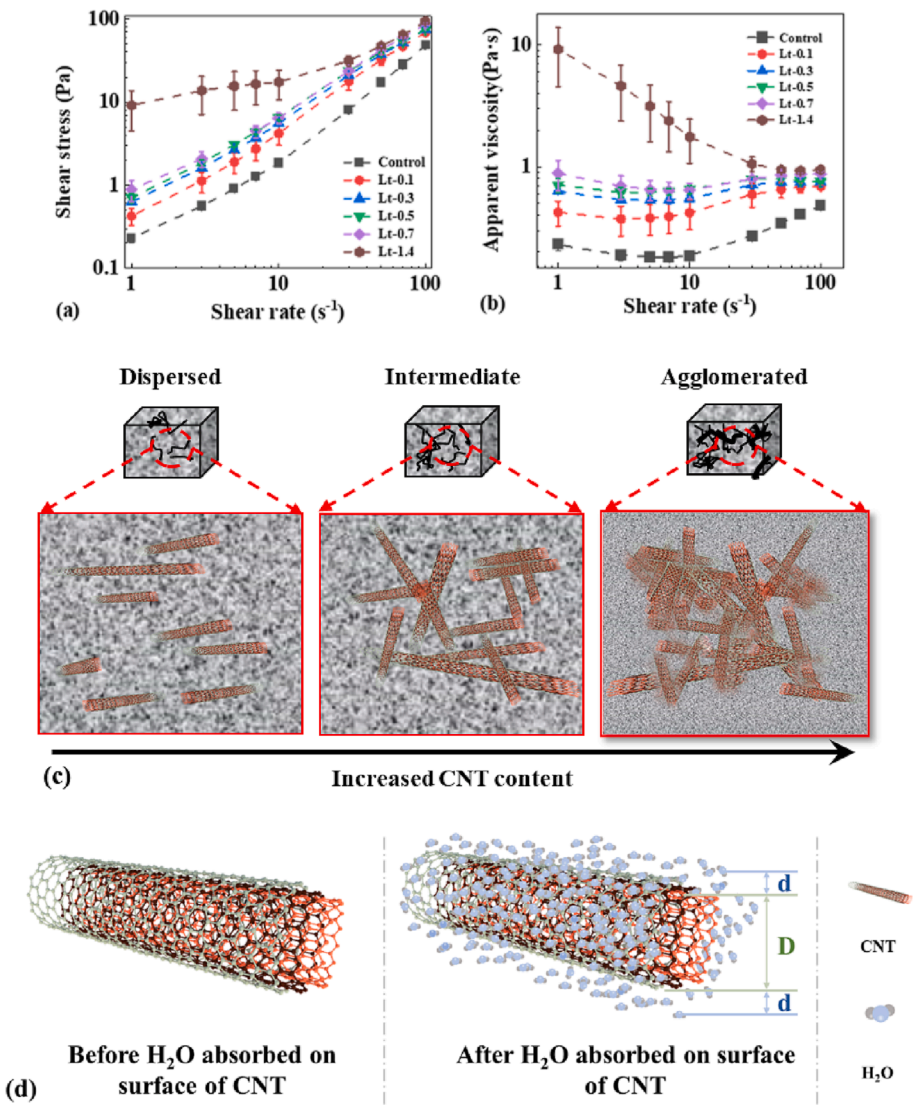

Fig. 4. Effects and mechanism of Lt content on the rheological behavior of cement pastes: (a)The shear stress-shear rate curves of cement pastes with Lt; (b) The apparent viscosity - shear rate curves of cement pastes with Lt; (c)The dispersion states of CNTs in the cement pastes with different contents of CNTs; (d) Schematic diagram of water adsorption of CNT in cement pastes.

free water is absorbed and trapped in the network structure of CNTs. The number and the volume of the network structure increases with the CNT content, as exhibited in Fig. 4 (c), Owing to the formation of an entangled CNT network, individual CNT motion is prevented [39], and thus a greater force is required to disperse CNTs, which in turn sharply increases the internal stress in cement pastes. Eventually, the apparent viscosities/shear stresses of cement pastes increase.

3.2. Rheological parameters

The yield stress (τ_0) has been determined in the flow curve (shear stress (τ) and shear rate (γ) in the range of 1 to 100 s^{-1}) based on the Herschel-Bulkley model [40] (Eq. (1)), which considers the accuracy and sensitivity of the yield stress [41]:

$$\tau = \tau_0 + K\dot{\gamma}^n \quad (1)$$

where τ is the shear stress (Pa), τ_0 is the yield stress (Pa), $\dot{\gamma}$ is the shear rate (s^{-1}), K is the consistency, and n is the flow index representing the degree of shear-thickening/shear-thinning ($n > 1/n < 1$). The yield stress and the flow index are shown in Fig. 5(a) and (c), respectively.

With the increasing shear rate, the apparent viscosity of cement pastes first decreases and then increases. The breakage of CNT aggregations as shear rate increase results in lower shear stress [28]. Therefore, a larger apparent viscosity has been observed in the low shear rate region (before the critical shear rate) for the cement paste with a fixed content of CNT. When the shear rate continues increasing, the viscosity of cement paste increases since clumps may form by extrusions between particles due to external hydrodynamic forces in highly anisotropic suspensions [42]. Obviously, there are the least interference factors for analyzing the inter-particle interactions between particles at the critical shear rate corresponding to the minimum viscosity . Therefore, the minimum viscosity at a critical shear rate is selected as an effective parameter to evaluate rheological behaviors of cement paste referring to [41], which can be identified in the shear rate region.

3.3. Effects of CNTs' length

Fig. 5 shows rheological parameters of cement pastes with four types of p-CNTs, i.e., LT, Lt, ST, and St.

The yield stress of cement paste with Lt is compared with that of cement paste with St at different CNT contents, as shown in Fig. 5(a).

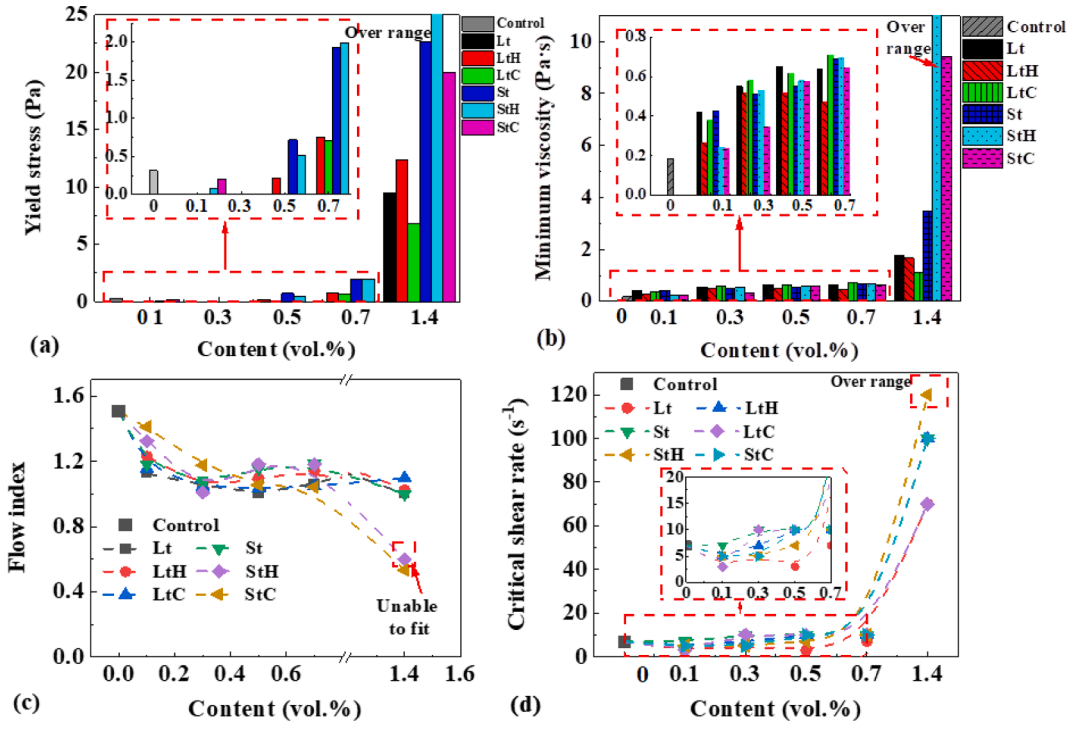

Fig. 5. The rheological parameters of cement pastes with different content of p-CNT (Lt/St), CNT-OH (LtH/StH), and CNT-COOH (LtC/StC): (a) Yield stress τ_0; (b) Minimum viscosity η_{min}; (c) Flow index n; (d) Critical shear rate..γ_{cri}

When the CNT content equals to or less than 0.3 vol%, the addition of CNTs slightly decreases the yield stresses of cement pastes. This may be associated with the increase of free water in the cement pastes by replacing the wrapped water in cement particles. When the CNT content ranges from 0.3 to 0.7 vol%, the yield stresses increase slowly with the increase of CNT content. When the CNT content increases from 0.7 to 1.4 vol%, the yield stresses of cement pastes with these two types of CNTs increase sharply, and the yield stresses of cement pastes with St are larger than that of cement pastes with Lt, i.e., $\tau_{0St} > \tau_{0Lt}$. However, the yield stresses of cement pastes containing ST are larger compared with that of the cement pastes containing LT, i.e., $\tau_{0ST} > \tau_{0LT}$. The minimum viscosities of cement pastes with four types of p-CNTs show similar trend with that of yield stresses, as shown in Fig. 5(b). The minimum viscosities of cement pastes with the four types of p-CNTs follow the trend of$\eta_{minSt} > \eta_{minLt}$ and $\eta_{minST} > \eta_{minLT}$, respectively.

In summary, the yield stresses and minimum viscosities of cement pastes with ST and St are larger than those of cement pastes with LT and Lt. This conclusion is different from that obtained in reference [43,44], and can be attributed the following three aspects. (1) The SSA of short CNTs (ST and St) is larger than that of long CNTs (LT and Lt) (Table 1), i.e., short CNTs have a stronger ability to adsorb free water at unit mass. This will decrease the distance between the CNTs, and facilitate the formation of entanglements between CNTs, increasing the interface friction between cement particles. (2) The zeta potential ζ (absolute value in Table 2) of ST/St is lower than that of LT/Lt, leading to that ST/St is easier to get agglomerations and form entanglements than LT/Lt. According to nanocomposite rheology theory [45], a greater force is required to disperse St, which in turn increases the internal stress in cement pastes. (3) The numbers and free water adsorption of ST/St with sub-micrometer at the same content is larger than that of LT/Lt with micrometer, which may facilitate a complex network structure formation in the cement paste and increase the friction between cement particles.

Fig. 5(c) shows the flow index n of cement pastes with four types of p-CNTs. The flow index n of cement paste with CNTs is smaller than that of the control, which means adding CNTs weakens the shear thickening degree of cement pastes. Fig. 5(d) shows the critical shear rate γ_{cri} of cement pastes with four types of p-CNTs. When the CNT content increases from 0.7 vol% to 1.4 vol%, the critical shear rate γ_{cri} of cement paste increases sharply. When the CNT content reaches 1.4 vol%, the critical shear rate of cement paste is in an order of $\gamma_{cri-St} > \gamma_{cri-ST} = \gamma_{cri-Lt} > \gamma_{cri-LT}$. This means the size of agglomerations and entanglements formed by CNTs in cement pastes are in an order of St > St ≈ LT > Lt.

3.4. Effects of CNTs' diameter

In this part, the effect of CNTs' diameter on the rheological behavior of cement paste is studied. First, the yield stress/minimum viscosity of cement paste with St and ST is compared, as shown in Fig. 5(a) and (b). It can be seen that when the content of St and ST is less than 0.7 vol%, the yield stresses/minimum viscosities of cement pastes are similar. By contrast, when the content exceeds 0.7 vol%, the yield stress/minimum viscosity of cement paste with St is much larger than that of cement paste with ST. Similarly, the yield stress/minimum viscosity of cement paste with Lt is larger than that of cement paste with LT. It can be seen from the above results CNTs with small diameter lead to a large yield stress/minimum viscosity of cement paste. The above results are related to the following two factors: (1) The aspect ratio of CNTs with small diameter is larger compared with that of large diameter and easier to be bent; (2) The amount of CNTs with small diameter is larger than that with large diameter at the same content, resulting in a more complex network structure formation of CNTs in cement pastes. This is consistent with the conclusion of Bounoua et al [46].

As shown in Fig. 5(c), the flow index of cement pastes with the small diameter CNT at the content of 1.4 vol% is less than that of cement pastes with the large diameter CNT, i.e., $n_{St} < n_{ST}$, $n_{Lt} < n_{LT}$. Fig. 5(d) demonstrates that the critical shear rates are similar in cement pastes containing different CNTs at the content less than 1.4 vol%, and the critical shear rates of cement pastes with four types of p-CNTs at the content of 1.4 vol% are in an order of $\gamma_{cri-St} > \gamma_{cri-ST}$, $\gamma_{cri-Lt} > \gamma_{cri-LT}$. The results indicate that more agglomerations and entanglements are formed

by CNTs with a smaller diameter in cement pastes.

3.5. Effects of CNTs' functionalization groups

3.5.1. Effects of the hydroxyl functionalization group of CNTs

Fig. 5 shows the rheological parameters of cement pastes with CNT-OH (StH and LtH). In particular, the rheological behavior of cement pastes with 1.4 vol% StH cannot be measured, because the cement paste system is so viscous that the rotor of the rheometer cannot be inserted into cement pastes for normal operation. Theoretically, the yield stress and minimum viscosity of cement pastes with StH are larger than that of cement paste with LtH, which conforms to the discipline identified in Section 3.2.1.

The yield stresses/minimum viscosities of cement pastes with CNT-OH (StH/LtH) are compared with cement pastes with p-CNTs (St/Lt) at different content levels, as shown in Fig. 5(a) and (b). When the content equals to or less than 0.7 vol%, the yield stress of cement paste with CNT-OH is similar with that of cement paste with p-CNTs. However, when the content >0.7 vol%, the yield stresses of cement pastes with CNT-OH are higher than that of cement pastes with p-CNTs. This may be related to the following two factors. (1) The presence of hydroxyl groups enhances the water absorption of CNTs [47], leading to low w/c ratio in local areas of cement pastes with CNT-OH and then increasing interaction between cement particles and CNTs, as well as promoting the formation of the network structure. (2) The cement paste is rich in Ca (OH)2, which affects the stability of CNT-OH suspensions and hinders the electrostatic repulsion between CNT-OH and SP, causing CNTs disperse worse [48].

The addition of CNT-OH decreases the flow index n of cement paste, as seen in Fig. 5(c). The value of n for cement paste with CNT-OH is larger than that of cement paste with the p-CNT. This may be attributed to the large water adsorption of CNT-OH to decreases the amount of free water that contributes to the fluidity of cement pastes, which facilitates the agglomerations of CNT-OH. Therefore, a higher critical shear rate (Fig. 5(d)) is required to break up the agglomerations of CNT-OH [19].

3.5.2. Effects of the carboxyl functionalization group of the CNTs

The yield stresses/minimum viscosities of cement pastes with CNT-COOH (StC/LtC) at different content levels are shown in Fig. 5(a) and (b). It can be seen that the yield stresses/minimum viscosities of cement pastes with CNT-COOH are smaller than that of cement pastes with the p-CNT. The yield stresses/minimum viscosities of cement pastes with StC, LtC, St, and Lt are in an order of St > StC > Lt > LtC. This phenomenon may be explained by two reasons: (1) The presence of -carboxyl functionalization grou has a positive impact on the dispersion of CNTs, which is conducive to the formation of additional stabilizing hydrogen bonds [49]; (2) High zeta potential of CNT-COOH renders the system a better dispersion as a result of electrostatic repulsion. Inferred from Table 2 that the electrostatic repulsion force of StC (the absolute value of Zeta potential is 29.9) is higher than that of St (20), indicating that StC can be better dispersed in cement pastes than St. The well-dispersed CNTs reduce the amount of "trapped water" in the network structure formed by the "entanglement effect" of CNTs in cement pastes and increase the free water to lower friction resistance between cement pastes.

The flow index n of cement paste with the p-CNTs (St/Lt) is larger than that of cement paste with CNT-COOH (LtC, StC), as exhibited in Fig. 5(c). It should be noted that the flow index of cement paste with 1.4 vol% StC is smaller than 1, implying that this kind of cement paste is a shear-thinning fluid. However, the flow index of cement paste with CNT-COOH (LtC, StC) lower than 1.4 vol% is >1, i.e., that this kind of cement paste is a shear-thickening fluid. Fig. 5 (d) shows that the critical shear rate of cement paste with p-CNT is similar to that of cement paste with CNT-COOH (LtC, StC). This indicates that the size of flocculation structure in cement pastes with CNT-COOH is similar to cement pastes with p-CNT.

3.5.3. Effects of different types of CNTs

The yield stress τ_0, the minimum viscosity η_{min}, the flow index n and the critical shear rate γ_{cri} of cement pastes with 1.4 vol% p-CNTs or functionalized CNTs are shown in Fig. 6.

Fig. 6 (a) shows that the yield stress τ_0 of cement pastes with different types of CNTs is in an order of $\tau_{0StH} > \tau_{0St} > \tau_{0StC} > \tau_{0LtH} > \tau_{0Lt} > \tau_{0LtC} > \tau_{0Control}$. When the length of CNTs is the same, the yield stresses of cement pastes with CNT-COOH are smaller than that of cement pastes with p-CNTs or CNT-OH. This is mainly because the zeta potential and dispersibility of CNT-COOH is larger than that of p-CNTs and CNT-OH. Besides, the water adsorption of CNT-OH is larger than that of p-CNTs and CNT-COOH, resulting in the largest water "adsorption effect" and the least free water in cement paste. In particular, the impact of water adsorption of CNTs on yield stress of cement paste is larger zeta potential.

Fig. 6(b) shows that the minimum viscosities η_{min} of cement pastes with different types of CNTs are in an order of $\eta_{minStH} > \eta_{minStC} > \eta_{minSt} > \eta_{minLtH} > \eta_{minLt} \approx \eta_{minLtC} > \eta_{minControl}$. The minimum viscosities of cement pastes with CNT-OH and CNT-COOH are larger than those of cement pastes with the p-CNTs, because CNTs with –COOH or –OH groups have strong interfacial bond adhesion with cement particles [50]. Furthermore, the long chains of –COOH or –OH groups of CNTs entangle with the increase of shear rate at the content of 1.4 vol%. The minimum viscosity of cement paste with CNT-COOH is smaller than that of cement paste with CNT-OH, because the –OH group can decrease the stability of CNTs suspension in cement paste. However, the minimum viscosity of cement paste with StC is larger than that of cement paste with St, while the minimum viscosity of cement paste with LtC is smaller than that of cement paste with Lt. This is attributed to the following two factors. On the one hand, the dispersibility of CNT-COOH is better than that of p-CNTs in cement paste [51]. On the other hand, the long chain of CNT-COOH with micrometer size is prone to entanglement, leading to remarkable "entanglement effect" at high contents and high shear rates. The combined effect of the above two factors contributes to the different results in minimum viscosity of cement paste with different length CNTs.

The flow index n of cement pastes with different types of CNTs is shown in Fig. 6(c). The flow index n of cement pastes with different types of CNTs is in an order of $n_{StC} < n_{StH} \approx n_{St} \approx n_{LtH} \approx n_{LtC} \approx n_{Lt} < n_{Control}$. The flow indexes of cement pastes containing CNTs are lower than that of the control cement pastes. The reasons have been discussed in the former of this section (Section 3.2.4.3).

The critical shear rate γ_{cri} of cement pastes with different CNTs is shown in Fig. 6(d). The critical shear rates γ_{cri} of cement pastes with StH, StC, St and LtH are the same, i.e., $\gamma_{criStH} = \gamma_{criStC} = \gamma_{criSt} = \gamma_{criLtH}$. At the same time, the above critical shear rates of these cement pastes are larger than that of cement pastes with LtC (γ_{criLtC}) and Lt (γ_{criLt}). The result shows that the critical shear rate of cement pastes with CNT-COOH and p-CNT are smaller than that of cement pastes with CNT-OH.

3.6. Viscosity prediction models of cement paste with CNTs

Cement paste is a kind of suspension. In the study of the rheological behavior of suspension, the relationships between the suspension viscosity (η) and particle volume fraction (ϕ) can be written as follow [52]:

$$\eta = \eta_0 \times f(\phi) \tag{2}$$

For cement paste with CNTs, $f(\phi) = f(\phi_c) \times f(\phi_{CNTs})$. Thus, Eq. (2) can be rewritten as Eq. (3):

$$\eta = \eta_0 \times f(\phi_c) \times f(\phi_{CNTs}) \tag{3}$$

where, ϕ_c is the volume fraction of cement particles; ϕ_{CNTs} is the volume fraction of CNTs. When the w/c ratio is fixed, the viscosity of cement paste with CNT is a function of ϕ_{CNTs}. However, the viscosity of the CNT suspension is too small to be measured by a certain rheometer. Therefore, it can be calculated by the ratio of the viscosity of cement paste

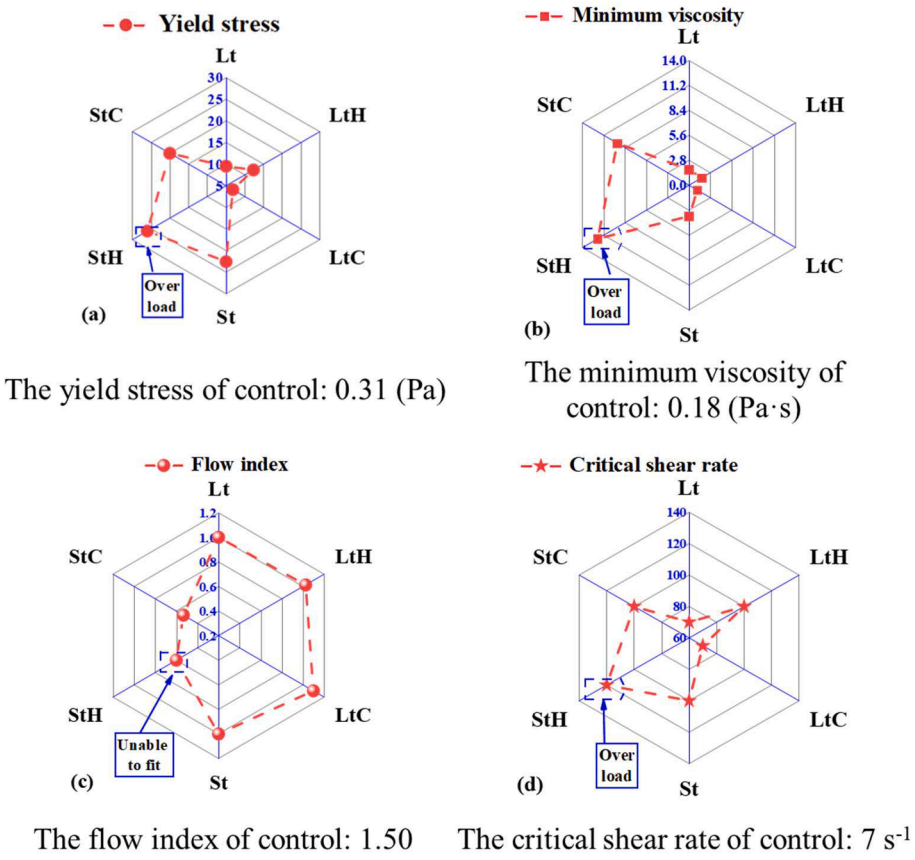

Fig. 6. Comparison of cement pastes containing various CNT with a diameter of 5 ~ 15 nm: (a) Yield stress τ_0; (b) Minimum viscosity η_{min}; (c) Flow index n; (d) Critical shear rate..γ_{cri}

with CNTs (η) and without CNTs (cement paste matrix, η_0), which is also called the relative viscosity (η_r), as shown in Eq. (4):

$$f(\phi_{CNTs}) = \frac{\eta}{\eta_0 \times f(\phi_c)} \tag{4}$$

3.6.1. The prediction of minimum viscosity of cement pastes with CNTs

In this section, the minimum viscosity of cement paste with CNTs is predicted. Einstein model [53] (Eq. (5)) and, Batchelor model [54] (Eq. (6)) and Brinkman model [55] (Eq. (7)), were usually used to reflect the relationships between relative viscosity and particle volume fraction (ϕ) [56]. The Einstein model [53] is used for very dilute suspensions (ϕ < 0.02) of perfectly rigid non-aggregating spheres in an incompressible fluid. The Batchelor model [54] considered the effects of Brownian motions, which is applicable for semi-dilute suspension. The Brinkman model [55] introduces (1 − ϕ) to account for the crowding effect of available particles, which is suitable for suspension with a medium particle volume fraction.

$$\eta_r = \frac{\eta}{\eta_0} = 1 + [\eta]\phi \tag{5}$$

$$\eta_r = 1 + 2.5\phi + 6.2\phi^2 \tag{6}$$

$$\eta_r = \frac{1}{(1-\phi)^{2.5}} \tag{7}$$

On the basis of results obtained in Section 3.2.1 ~ 3.2.4, rheological behaviors of cement pastes with CNTs are affected by "adsorption effect" and "entanglement effect" simultaneously. Considering the effect of CNT water adsorption (actually, also a part of the volume exclusion effect, which is related to the length, diameter as well as functional groups of CNTs), the effective volume fraction (ϕeff)is used to simply modify the classical equations, as shown in Eq. (8):

$$\phi_{eff} = k\phi \tag{8}$$

where the coefficient k (>1) represents the magnification of CNT volume is mainly due to water absorption. Based on the relationship between k and ϕ_{eff} above-mentioned, the coefficient k is related to the length, diameter as well as functional groups of CNTs. The water absorption effect of CNTs can be illustrated in Fig. 4(d). Due to the high aspect ratio of CNTs, the water adsorbed at the port of CNTs can be ignored. Therefore, the CNT volume amplification coefficient k can be calculated by the following Equation:

$$\mathrm{k} = \frac{n \times \pi \times (\frac{D}{2} + \mathrm{d})^2 \times l}{n \times \pi \times (\frac{D}{2})^2 \times l} = (1 + \frac{2d}{D})^2 \tag{9}$$

where d (>0) is the water adsorption thickness of CNTs. Thus, the effective volume fraction (ϕ_{eff}) mainly caused by the water adsorption can be rewritten as Eq. (10):

$$\phi_{eff} = \left(1 + \frac{2d}{D}\right)^2 \times \phi \tag{10}$$

In this section, the minimum viscosities of cement pastes with CNTs are predicted by the modified classical viscosity prediction models (Table 6) based on the effective volume fraction (ϕ_{eff}) of CNTs. The prediction results of the relative viscosity (ηr)have low accuracy, as shown in Table 6.

Thus, the viscosity prediction model should be further modified. The CNTs content (0 ~ 1.4 vol%) in this experiment is within the range of the solute particle volume content of the dilute solution (ϕ less than 2 %), which meets the content variation range of the Einstein model.

The viscosity prediction model for cement paste with CNTs are

Table 6
The modified classical viscosity prediction models.

The modified classical viscosity prediction models	The modified classical viscosity prediction equation	Equation
Modified Einstein model	$\eta_r = \frac{\eta}{\eta_0} = 1 + [\eta]\phi_{eff}$	(11)
Modified Batchelor model	$\eta_r = 1 + 2.5\phi_{eff} + 6.2\phi_{eff}^2$	(12)
Modified Brinkman model	$\eta_r = \frac{1}{\left(1-\phi_{eff}\right)^{2.5}}$	(13)

established according to previous modified Einstein viscosity prediction model (Eq. (11)) and the modification mechanisms of CNTs. Because the content of CNTs (ϕ) is close to 0, the modified Einstein model (Eq. (11)) can be rewritten as Eq. (14) to predict viscosity of cement pastes with CNTs less than 1.4 vol%.

$$\eta_r = 1 + [\eta]\phi_{eff} = 1 + \left[1 + \phi_{eff}^{[\eta]} - 1\right] = 1 + \phi_{eff}^{[\eta]} \tag{14}$$

In Eq. (14), parameter ([η])is used to describe the formation kinetics of the network structure of CNTs, which is influenced by the length, diameter, and functional groups of CNTs in cement pastes. A larger [η] indicates that the network structure of CNTs in cement paste is formed faster.

3.6.2. Prediction results and accuracy

Table 7 shows the fitting results of ηr based on modified classical models and the author's model proposed in Section 3.2.5.2. Obviously, the fitted ηr of proposed model based on the "adsorption effect" and "entanglement effect" of CNTs is more accurate than the fitted results of the other three modified classical models, as shown in Table 8.

According to Eq. (8) ~ (10), the water film adsorption thickness *d* of an individual CNT (as shown in Fig. 4(d)) can be calculated. The corresponding results are shown in Table 9.

The water film adsorption thickness *d* is calculated to be positive for all types of CNTs, as the results are fitted by the author's model. Because the amplification coefficient *k* is directly introduced on the basis of the classical model to characterize the amplification of volume mainly owning to the adsorption of water. Therefore, the difference of the water film thickness obtained in different models mainly reflects the adaptability of the volume amplification coefficient k to the viscosity models under this assumption. The obtained water film thickness conforms to the actual situation, which indicates that the amplification factor *k* is more appropriate in this kind of model. However, the fitted results for *d* in the other three models are negative sometimes, which violates the assumption (d > 0) in this study. The above results prove the reasonable of the new proposed viscosity prediction model. Hence, the minimum viscosity prediction model of cement pastes with CNTs can be calculated by Eq. (15):

$$\eta = \eta_0 \times \eta_{r\ \phi_{MWCNT}/c} = \eta_0 \times \left(1 + \left(k \times \phi_{CNT/C}\right)^{[\eta]}\right) \tag{15}$$

here η0 represents the minimum viscosity of cement paste without CNTs. The relationship between $\phi_{CNTs/W}$ and $\phi_{CNTs/C}$ (the ratio of CNT particle volume to cement particle volume) can be calculated by Eq. (16):

$$\phi_{CNTs/W} = \frac{V_C}{V_W} \times \phi_{CNTs/C} \tag{16}$$

where, $\frac{V_C}{V_W}$ is the ratio of the volume of water to cement particles. It can be calculated via Eq. (17):

$$\frac{V_C}{V_W} = \frac{m_C/\rho_C}{m_W/\rho_W} = \frac{\rho_W/\rho_C}{m_W/m_C} \tag{17}$$

where m_C is the mass of cement; m_W is the mass of the water; ρ_C is the density of cement, which is equal to 3.1 g/cm^3; ρ_W is the density of water, which is equal to 1 g/cm^3; and the m_W/m_C = w/c ratio = 0.24.

For cement paste with a certain content of CNTs, Eq. (15) can be rewritten as Eq. (18), and the specific equation are shown in Table 10:

The parameters in Table 10 is fitted by the proposed model in Eq. (15). In Eq. (15), a large parameter *k* and [η] is related to large water adsorption ability and large network structure formation ability of CNTs in cement paste, respectively. This makes the cement paste is more difficult to mix and the grouting flow rate is slower as well as the cement paste is harder to compact. Additionally, it can be seen from the above Equations (18-1) ~ (18-8) that cement pastes containing CNTs with micrometer length, large diameter, and functionalization groups show a larger volume magnification coefficient k, indicating that these CNTs have a much thicker water film. The cement pastes containing CNTs with sub-micrometer length, small diameter, and functionalization groups show a large parameter [η], representing that these CNTs in cement pastes will form the network structure fast. At the same time, it can be seen that the length and diameter of CNTs mainly affect their "entanglement effect", while functionalization groups affect both "entanglement effect" and "adsorption effect" in cement pastes. Moreover, as the content increases, the rate of network structure formation of CNTs is greater than that of water adsorption. The proposed model considers the both effects of both water adsorption and CNT network structure, thereby improving the accuracy of viscosities prediction model for cement paste with different types and contents of CNTs.

4. Conclusions

The effects of physicochemical properties of CNTs, including length, diameter, and functionalization groups, on rheological behaviors of cement pastes are systematically investigated in this study. The rheological parameters of CNTs modified cement paste such as yield stress,

Table 7
The fitting results of η_r based on classical models and the author's model.

CNT	Prediction results of cement paste with different models								
	Modified Einstein model $\eta_r = \frac{\eta}{\eta_0} = 1 + 2.5\phi_{eff}$		Modified Brinkman model $\eta_r = \frac{1}{(1-\phi_{eff})^{2.5}}$		Modified Batchelor model $\eta_r = 1 + 2.5\phi_{eff} + 6.2(\phi_{eff})^2$		Author' model $\eta_r = 1 + (\phi_{eff})^{[\eta]}$		
	k	R^2	k	R^2	k	R^2	k	a	R^2
St	2.26	0.81	0.58	0.96	0.27	0.98	1.34	2.36	0.98
ST	0.98	0.65	0.32	0.15	0.21	-0.25	3.72	0.75	0.79
StH	7.37	0.69	1.14	0.92	0.32	0.99	1.05	4.26	0.99
StC	5.79	0.70	1.00	0.92	0.31	0.99	1.04	4.03	0.99
Lt	1.05	0.82	0.37	0.86	0.23	0.81	1.57	1.46	0.82
LT	0.35	0.88	0.17	0.81	0.15	0.75	1.61	0.83	0.87
LtH	1.14	0.89	0.39	0.94	0.24	0.77	1.59	1.52	0.93
LtC	0.86	0.87	0.30	0.58	0.21	0.30	4.96	0.62	0.98

Note, η_r is the relative viscosity; η *is* suspension viscosity; η_0 is suspending medium (cement paste without CNTs); ϕ_{eff} is the effective volume fraction of CNTs.

Table 8
The fitting results of η_r based on modified classical models and the author's model.

Viscositypredictionmodel	Content (vol.%)	Fitted η_r of St	Regular Residual of "η_r"	Fitted η_r of ST	Regular Residual of "η_r"	Fitted η_r of StH	Regular Residual of "η_r"	Fitted η_r of StC	Regular Residual of "η_r"	Fitted η_r of Lt	Regular Residual of "η_r"	Fitted η_r of LT	Regular Residual of "η_r"	Fitted η_r of LtH	Regular Residual of "η_r"	Fitted η_r of LtC	Regular Residual of "η_r"
Modified Einstein model	0	1	0	1	0	1	0	1	0	1	0	1	0	1	0	1	0
	0.1	2.02	0.29	1.44	0.97	4.33	−3.02	3.61	−2.33	1.47	0.80	1.16	0.45	1.52	−0.078	1.39	0.67
	0.3	4.06	−1.29	2.33	1.59	10.99	−8.11	8.84	−6.97	2.41	0.57	1.48	0.2	2.55	0.27	2.16	0.98
	0.5	6.1	−3.11	3.22	1.11	17.64	−14.5	14.07	−10.94	3.36	0.16	1.79	0.08	3.58	−0.79	2.94	0.4
	0.7	8.15	−4.4	4.1	0.31	24.3	−20.54	19.30	−15.8	4.31	−0.84	2.11	−0.28	4.61	−2.06	3.71	0.13
	1.4	15.29	3.57	7.20	−0.96	47.6	17.4	37.59	13.47	7.61	1.91	3.23	0.04	8.21	0.85	6.43	−0.47
Modified Batchelor model	0	1	0	1	0	1	0	1	0	1	0	1	0	1	0	1	0
	0.1	1.33	0.97	1.17	1.25	1.78	−0.47	1.66	−0.38	1.19	1.08	1.09	0.53	1.2	0.23	1.16	0.89
	0.3	2.4	0.37	1.63	2.29	4.94	−2.06	4.19	−2.33	1.75	1.24	1.3	0.38	1.8	1.01	1.58	1.56
	0.5	4.02	−1.02	2.26	2.07	10.21	−7.07	8.36	−5.24	2.52	1	1.56	0.32	2.64	0.15	2.16	1.19
	0.7	6.18	−2.44	3.06	1.35	17.61	−13.84	14.16	−10.67	3.51	−0.04	1.87	−0.04	3.73	−1.18	2.88	0.96
	1.4	18.06	0.81	7.2	−0.96	60.19	4.81	47.31	3.76	8.71	0.81	3.36	−0.1	9.46	−0.39	6.6	−0.64
Modified Brikman model	0	1	0	1	0	1	0	1	0	1	0	1	0	1	0	1	0
	0.1	1.14	1.17	1.17	1.25	1.16	0.15	1.16	0.12	1.12	1.16	1.07	0.54	1.12	0.32	1.1	0.95
	0.3	1.49	1.28	1.63	2.29	1.61	1.26	1.59	0.28	1.41	1.58	1.24	0.43	1.41	1.39	1.34	1.8
	0.5	2.03	0.96	2.26	2.07	2.35	0.79	2.3	0.83	1.82	1.7	1.45	0.44	1.83	0.96	1.67	1.67
	0.7	2.88	0.85	3.06	1.35	3.68	0.09	3.53	−0.04	2.43	1.04	1.71	0.13	2.45	0.09	2.13	1.71
	1.4	18.92	−0.06	7.2	−0.97	65.01	−0.01	51.06	0	9.79	−0.27	3.36	−0.1	10.1	−1.03	6.29	−0.33
Author's model	0	1	0	1	0	1	0	1	0	1	0	1	0	1	0	1	0
	0.1	1.04	1.27	1.74	0.67	1	0.31	1	0.31	1.16	1.11	1.5	0.11	1.15	0.29	1.93	0.11
	0.3	1.47	1.3	2.69	1.23	1.09	1.78	1.09	1.78	1.79	1.2	1.93	−0.25	1.8	1.01	2.85	0.3
	0.5	2.57	0.43	3.48	0.84	1.8	1.34	1.8	1.34	2.66	0.86	2.23	−0.35	2.73	0.06	3.54	−0.19
	0.7	4.47	−0.73	4.195	0.21	4.34	−0.58	4.35	−0.58	3.71	−0.24	2.48	−0.65	3.88	−1.34	4.13	−0.29
	1.4	18.8	0.07	6.37	−0.13	64.99	0.01	64.99	0.01	8.44	1.08	3.17	0.09	9.26	−0.19	5.81	0.15
Test data	0	1	/	1	/	1	/	1	/	1	/	1	/	1	/	1	/
	0.1	2.30	/	2.41	/	1.31	/	1.28	/	2.28	/	1.61	/	1.44	/	2.05	/
	0.3	2.78	/	3.92	/	2.87	/	1.87	/	2.99	/	1.67	/	2.81	/	3.15	/
	0.5	2.30	/	4.33	/	3.14	/	3.13	/	3.52	/	1.88	/	2.79	/	3.35	/
	0.7	3.75	/	4.41	/	3.76	/	3.50	/	3.47	/	1.83	/	2.55	/	3.84	/
	1.4	18.87	/	6.24	/	65.01	/	51.06	/	9.52	/	3.26	/	9.07	/	5.96	/

Table 9
The thickness of absorbed water-film calculated by various viscosity prediction models.

The thickness of absorbed water-film d (nm)	Modified Einstein model	Modified Batchelor model	Modified Brikman model	Author's model
St	2.366461	−1.11776	−2.24245	0.739605
ST	−0.10554	−4.74099	−5.95504	10.21603
StH	8.059837	0.328212	−2.03738	0.116285
StC	6.606139	0.008642	−2.06889	0.102342
Lt	0.106937	−1.84698	−2.41379	1.182663
LT	−4.47342	−6.37138	−6.71158	2.944599
LtH	0.319607	−1.76895	−2.40423	1.223382
LtC	−0.34466	−2.10623	−2.56708	5.767172

Table 10
Viscosity prediction of cement pastes with CNTs.

CNTs	Author's model for individual mixtures $\eta = \eta_0 \times (1 + (k \times \phi_{CNT/C})^{[\eta]})$	Equation
St	$\eta = 0.1846 \times (1 + (1.34\phi)^{2.36})$	(18-1)
ST	$\eta = 0.1846 \times (1 + (3.72\phi)^{0.75})$	(18-2)
StH	$\eta = 0.1846 \times (1 + (1.05\phi)^{4.26})$	(18-3)
StC	$\eta = 0.1846 \times (1 + (1.04\phi)^{4.03})$	(18-4)
Lt	$\eta = 0.1846 \times (1 + (1.57\phi)^{1.46})$	(18-5)
LT	$\eta = 0.1846 \times (1 + (1.61\phi)^{0.83})$	(18-6)
LtH	$\eta = 0.1846 \times (1 + (1.59\phi)^{1.52})$	(18-7)
LtC	$\eta = 0.1846 \times (1 + (4.96\phi)^{0.62})$	(18-8)

minimum viscosity, flow index, and critical shear rate were analyzed and the minimum viscosity prediction model was established based on the "adsorption effect" and "entanglement effect" of MWNCTs. The following conclusions can be drawn:

(1) The yield stress and minimum viscosity of cement pastes containing CNTs with sub-micron length and diameter of 5 ~ 15 nm are larger than those of cement pastes containing CNTs with micrometer length and diameter of 20 ~ 30 nm. This is mainly affected by the "entanglement effect" effect of CNTs. With the increase of the CNT content, the flow index of cement paste decreases, while the critical shear rate increases significantly.
(2) The yield stress and minimum viscosity of CNT-OH modified cement paste are larger than that of p-CNT modified cement paste due to the large water adsorption of CNT-OH. By contrast, the yield stress and minimum viscosity of cement paste with CNT-COOH are smaller than that of cement paste with the p-CNTs at most contents as a result of larger zeta potential.
(3) The viscosity prediction model considering "adsorption effect" and "entanglement effect" of CNT is firstly proposed for cement paste with different types and contents of CNTs. The accuracy of the proposed viscosity prediction model is higher than that of the modified classical viscosity prediction models. Furthermore, it provided a direction of the workability of cement paste with different CNTs.

CRediT authorship contribution statement

Hongyan Li: Methodology, Validation, Formal analysis, Investigation, Writing – original draft, Writing – review & editing. **Zhenming Li:** Methodology, Investigation, Writing – original draft. **Liangsheng Qiu:** Methodology, Investigation. **Sufen Dong:** Investigation, Writing – review & editing, Supervision, Project administration, Funding acquisition. **Jian Ouyang:** Methodology, Supervision. **Xufeng Dong:** Methodology, Supervision. **Baoguo Han:** Conceptualization, Resources, Writing – original draft, Writing – review & editing, Supervision, Project administration, Funding acquisition.

Declaration of Competing Interest

The authors declare that they have no known competing financial interests or personal relationships that could have appeared to influence the work reported in this paper.

Data availability

All data has been included in the submitted manuscript

Acknowledgment

The authors would like to thank the National Science Foundation of China (52178188, 51908103 and 51978127), the Fundamental Research Funds for the Central Universities (DUT21RC (3)039) for providing funding to carry out this investigation.

References

[1] H. Fan, H. Wang, N. Zhao, et al., Hierarchical nanocomposite of polyaniline nanorods grown on the surface of carbon nanotubes for high-performance supercapacitor electrode, J. Mater. Chem. 22 (6) (2012) 2278–2774.
[2] X. Yao, C. Wu, H. Wang, et al., Effects of carbon nanotubes and metal catalysts on hydrogen storage in magnesium nanocomposites, J. Nanosci. Nanotechnol. 6 (2) (2006) 494–498.
[3] B. Han, S. Ding, J. Wang, et al., Nano-engineered cementitious composites: principles and practices, Springer, Singapore, 2019.
[4] S. Ding, X. Wang, L. Qiu, et al., Self-sensing cementitious composites with hierarchical carbon fiber-carbon nanotube composite fillers for crack development monitoring of a maglev girder, Small 19 (2023) 2206258.
[5] M. Mohsen, R. Taha, A. Abu Taqa, et al., Effect of nanotube geometry on the strength and dispersion of CNT-cement composites, J. Nanomater. 2017 (2017) 1–15.
[6] D. Lu, X. Shi, J. Zhong, Understanding the role of unzipped carbon nanotubes in cement pastes, Cem. Concr. Compos. 126 (2022), 104366.
[7] S. Ding, Y. Xiang, Y. Ni, et al., In-situ synthesizing carbon nanotubes on cement to develop self-sensing cementitious composites for smart high-speed rail infrastructures, Nano Today 43 (2022), 101438.
[8] B. Liang, Z. Lin, W. Chen, et al., Ultra-stretchable and highly sensitive strain sensor based on gradient structure carbon nanotubes, Nanoscale 10 (28) (2018) 13599–13606.
[9] A. Singh, B. Gupta, M. Mishra, et al., Multiwalled carbon nanotube/cement composites with exceptional electromagnetic interference shielding properties, Carbon 56 (2013) 86–96.
[10] I. Nam, H. Kim, H. Lee, Influence of silica fume additions on electromagnetic interference shielding effectiveness of multi-walled carbon nanotube/cement composites, Constr. Build. Mater. 30 (2012) 480–487.
[11] W. Li, W. Ji, Y. Liu, et al., Damping property of a cement-based material containing carbon nanotube, J. Nanomater. 12 (2015), 371404.
[12] S. Jiang, B. Shan, J. Ouyang, et al., Rheological properties of cementitious composites with nano/fiber fillers, Constr. Build. Mater. 158 (2018) 786–800.
[13] B. Boulekbache, M. Hamrat, M. Chemrouk, et al., Flowability of fiber-reinforced concrete and its effect on the mechanical properties of the material, Constr. Build. Mater. 24 (9) (2010) 1664–1671.
[14] A. Rashad, An overview on rheology, mechanical properties and durability of high-volume slag used as a cement replacement in paste, mortar and concrete, Constr. Build. Mater. 187 (2018) 89–117.
[15] T. Ponikiewski, J. Gołaszewski, Properties of steel fiber reinforced self-compacting concrete for optimal rheological and mechanical properties in precast beams, Procedia Eng. 65 (2013) 290–295.
[16] Banfill P. The rheology of fresh cement and concrete-a review. Proceedings of the 11th international cement chemistry congress: 2003:50-62.
[17] D. Leonavičius, I. Pundienė, G. Girskas, et al., The influence of carbon nanotubes on the properties of water solutions and fresh cement pastes, IOP Conference Series: Materials Science and Engineering 251(1):12023 (2017).
[18] D. Leonavičius, I. Pundienė, G. Girskas, et al., The effect of multi-walled carbon nanotubes on the rheological properties and hydration process of cement pastes, Constr. Build. Mater. 189 (2018) 947–954.
[19] G. Skripkiunas, E. Karpova, I. Barauskas, et al., Rheological properties of cement pastes with multiwalled carbon nanotubes, Adv. Mater. Sci. Eng. 2018 (2018) 1–13.
[20] O. Mendoza Reales, Y. Arias Jaramillo, J. Ochoa Botero, et al., Influence of MWCNT/surfactant dispersions on the rheology of Portland cement pastes, Cem. Concr. Res. 107 (2018) 101–109.
[21] J. De Paula, J. Calixto, L. Ladeira, et al., Mechanical and rheological behavior of oil-well cement slurries produced with clinker containing carbon nanotubes, J. Pet. Sci. Eng. 122 (2014) 274–279.
[22] T. Qureshi, D. Panesar, Nano reinforced cement paste composite with functionalized graphene and pristine graphene nanoplatelets, Compos. B Eng. 197 (2020), 108063.

[23] L. Assi, A. Alsalman, D. Bianco, et al., Multiwall carbon nanotubes (MWCNTs) dispersion & mechanical effects in OPC mortar & paste: a review, Journal of Building Engineering 43 (2021), 102512.
[24] Y. Cao, P. Zavaterri, J. Youngblood, et al., The influence of cellulose nanocrystal additions on the performance of cement paste, Cem. Concr. Compos. 56 (2015) 73–83.
[25] L. Zhao, X. Guo, Y. Liu, et al., Investigation of dispersion behavior of GO modified by different water reducing agents in cement pore solution, Carbon 127 (2018) 255–269.
[26] Y. Huang, S. Ahir, E. Terentjev, Dispersion rheology of carbon nanotubes in a polymer matrix, Phys. Rev. B 73 (12) (2006).
[27] A. Nasiri, M. Shariaty-Niasar, A. Rashidi, et al., Effect of dispersion method on thermal conductivity and stability of nanofluid, Exp. Therm Fluid Sci. 35 (4) (2011) 717–723.
[28] K. Soma, J. Babu, Factors influencing the rheological behavior of carbon nanotube water-based nanofluid, Fullerenes, Nanotubes, Carbon Nanostruct. 23 (8) (2015) 750–754.
[29] F. Collins, J. Lambert, W. Duan, The influences of admixtures on the dispersion, workability, and strength of carbon nanotube–OPC paste mixtures, Cem. Concr. Compos. 34 (2) (2012) 201–207.
[30] T. Yokozeki, S. Carolin Schulz, S. Buschhorn, et al., Investigation of shear thinning behavior and microstructures of MWCNT/epoxy and CNF/epoxy suspensions under steady shear conditions, Eur. Polym. J. 48 (6) (2012) 1042–1049.
[31] W. Ma, F. Chinesta, A. Ammar, et al., Rheological modeling of carbon nanotube aggregate suspensions, J. Rheol. 52 (6) (2008) 1311–1330.
[32] W. Ma, F. Chinesta, M. Mackley, et al., The rheological modelling of carbon nanotube (CNT) suspensions in steady shear flows, Int. J. Mater. Form. 1 (2) (2008) 83–88.
[33] J. Hong, I. Hong, H. Lim, et al., In situ lubrication dispersion of multi-walled carbon nanotubes in poly(propylene) melts, Macromol. Mater. Eng. 297 (3) (2012) 279–287.
[34] P. Pötschke, T. Fornes, D. Paul, Rheological behavior of multiwalled carbon nanotube/polycarbonate composites, Polymer 43 (11) (2002) 3247–3255.
[35] F. Du, R. Scogna, W. Zhou, et al., Nanotube networks in polymer nanocomposites: rheology and electrical conductivity, Macromolecules 37 (24) (2004) 9048–9055.
[36] M. Shaffer, X. Fan, A. Windle, Dispersion and packing of carbon nanotubes, Carbon 36 (11) (1998) 1603–1612.
[37] K. Yearsley, M. Mackley, F. Chinesta, et al., The rheology of multiwalled carbon nanotube and carbon black suspensions, J. Rheol. 56 (6) (2012) 1465–1490.
[38] Y. Zare, H. Garmabi, K. Rhee, Structural and phase separation characterization of poly (lactic acid)/poly (ethylene oxide)/carbon nanotube nanocomposites by rheological examinations, Compos. B Eng. 144 (2018) 1–10.
[39] I. Kinloch, S. Roberts, A. Windle, A rheological study of concentrated aqueous nanotube dispersions, Polymer 43 (26) (2002) 7483–7491.
[40] F. Larrard, C. Ferraris, T. Sedran, Fresh concrete: A Herschel-Bulkley material, Mater. Struct. 31 (7) (1998) 494–498.
[41] H. Li, S. Ding, L. Zhang, et al., Effects of particle size, crystal phase and surface treatment of nano-TiO_2 on the rheological parameters of cement paste, Constr. Build. Mater. 239 (2020), 117897.
[42] C. Schmid, D. Klingenberg, Mechanical flocculation in flowing fiber suspensions, Phys. Rev. Lett. 84 (2) (2000) 290–293.
[43] S. Shen, S. Bateman, C. Huynh, et al., Impact of carbon nanotube aspect ratio and dispersion on epoxy nanocomposite performance, Adv. Mat. Res. 66 (2009) 198–201.
[44] S. Iwamoto, S. Lee, T. Endo, Relationship between aspect ratio and suspension viscosity of wood cellulose nanofibers, Polym. J. 46 (1) (2014) 73–76.
[45] D. Litchfield, D. Baird, The rheology of high aspect ratio nano-particle filled liquids, Rheology Reviews. 2006 (2006) 1.
[46] S. Bounoua, E. Lemaire, J. Férec, et al., Shear-thinning in concentrated rigid fiber suspensions: Aggregation induced by adhesive interactions, J. Rheol. 60 (6) (2016) 1279–1300.
[47] X. Sun, Q. Wu, S. Lee, et al., Cellulose nanofibers as a modifier for rheology, curing and mechanical performance of oil well cement, Sci. Rep. 6 (1) (2016) 31654.
[48] O. Mendoza, G. Sierra, J. Tobón, Influence of super plasticizer and Ca $(OH)_2$ on the stability of functionalized multi-walled carbon nanotubes dispersions for cement composites applications, Constr. Build. Mater. 47 (2013) 771–778.
[49] B. Jóźwiak, S. Boncel, Rheology of ionanofluids – A review, J. Mol. Liq. 302 (2020), 112568.
[50] R. Rao, B. Sindu, S. Sasmal, Synthesis, design and piezo-resistive characteristics of cementitious smart nanocomposites with different types of functionalized MWCNTs under long cyclic loading, Cem. Concr. Compos. 108 (2020), 103517.
[51] I. Amr, A. Al-Amer, S. Thomas-P, et al., Effect of acid treated carbon nanotubes on mechanical, rheological and thermal properties of polystyrene nanocomposites, Compos. B Eng. 42 (6) (2011) 1554–1561.
[52] J. Ouyang, B. Han, G. Cheng, et al., A viscosity prediction model for cement paste with nano-SiO_2 particles, Constr. Build. Mater. 185 (2018) 293–301.
[53] A. Einstein, Investigations on the theory of the Brownian movement, Courier Corporation, 1956.
[54] G. Batchelor, The stress generated in a non-dilute suspension of elongated particles by pure straining motion, J. Fluid Mech. 46 (4) (1971) 813–829.
[55] H. Brinkman, The viscosity of concentrated suspensions and solutions, J. Chem. Phys. 20 (4) (1952) 571.
[56] Y. Song, Q. Zheng, Concepts and conflicts in nanoparticles reinforcement to polymers beyond hydrodynamics, Prog. Mater Sci. 84 (2016) 1–58.